Dust around (long-period) classical cepheids

Martin A.T. Groenewegen

Koninklijke Sterrenwacht van België, Belgium

The Introduction

Classical Cepheids (CCs) are an important standard candle because they are bright and provide a link between the distance scale in the nearby universe and that further out via those galaxies that contain both Cepheids and SNIa (see Riess et al. 2022 for a determination of the Hubble constant to 1.0 km s^{-1} precision). Typically, the period-luminosity (PL) relations of CCs that are at the core of the distance determinations are derived in particular photometric filters (V, I, K) or combination of filters that are designed to be reddening independent, the so-called Wesenheit functions (Madore 1982), e.g. using combinations of (V, I), (J, K), or the combination used by the SH0ES program (F555W, F814W, and F160W HST filters, see Riess et al. 2022).
On the other hand, the bolometric magnitude or luminosity is a fundamental quantity of CCs and stars in general as it is the output of stellar evolution models and the input to CC pulsation models. In Groenewegen (2020, hereafter G20) the spectral energy distributions (SEDs) of 477 Galactic CCs were constructed and fitted with model atmospheres (and a dust component when required). For an adopted distance and reddening these fits resulted in a best-fitting bolometric luminosity (L; for an adopted distance and reddening) and the photometrically derived effective temperature ($T_{\rm eff}$).
For about 20 objects an additional dust component was indeed required to fit the SED, including a dozen for which there are mid-IR spectra available to constrainthe dust composition. Near- and mid-IR excess is known to exist in Galactic CCs, for example, via direct interferometric observations in the optical or NIR (e.g. Kervella et al. 2006, Merand et al. 2006, Gallenne et al. 2012, Nardetto et al. 2016), modelling with the SPIPS code (e.g. Breitfelder et al. 2016, Trahin 2019, Trahin et al. 2021, and Gallenne et al. 2017 for the LMC) and was also found in modelling of the SEDs of Galactic CCs (Gallenne et al. 2013, G20). Performing a best fit to to the SED with a dust component or only a model atmosphere (and marking any formally deviant points in the MIR as outliers) can result in changes in the best-fitting values of L and $T_{\rm eff}$ and systematic changes in the predicted magnitudes. In a model with dust the IR magnitudes become brighter, and because dust absorps radiation, fainter in the optical. Generally this is true but when a full fit is done and L is allowed to vary the predicted magnitudes can be brighter also in the optical (see examples in Table 3 in G20 and Table 3 in GL23).
Groenewegen & Lub (2023, hereafter GL23) performed a similar study on the SEDs of 142 Large Magellanic Cloud (LMC) and 77 Small Magellanic Cloud (SMC) fundamental-mode (FM) CCs. Only one convincing example of a star with an IR excess was found, namely the CC with the longest period in the LMC sample (133 d).
Is the presence of IR excess related to period and/or to metallicity ? The effect of dust can be a few hundreth of a magnitude and is typically not considered as a source of systematic uncertainty in the calibration of the Cepheid PL-relation.
This poster presents preliminary results on a systematic study of long-period ($P > 50$ d) CCs in nearby galaxies to investigate this; a paper describing this research in detail is in preparation. This study is connected to the class of ultra long-period (ULP) cepheids, a term introduced by Bird et al. (2009) as FM cepheids with periods longer than 80 days (see reviews by Musella et al. (2021) and Musella (2022) specifically on ULPs).

The Sample

In this paper a sample of 55 cepheids are studied. In particular the sample is composed of

- Galactic cepheids from Pietrukowicz et al. (2021) which contains 3666 CCs (status September 2022) The longest period listed there is S Vul with a period of 68.65 d, clearly shorter than the classical limit of 80 days for ULPs. An (arbitrary) lower limit of 50 days will be used, which results in nine objects.
- SMC and LMC CCs from the OGLE-IV catalogue Soszynski et al. (2019), resulting in six and eight objects, respectively, with periods longer than 50 days.
- From the *Gaia* DR3 `vari_cepheid` table all CCs with a period longer than 50 days and type DCEP were selected, for a total of 53 objects (Ripepi et al. 2023).

All of the sources from Pietrukowicz et al. (2021) are in the `vari_cepheid` table, except OGLE-GD-CEP-1505. It is listed there but classified as a Type-II cepheid (T2C) of the RV Tau class. It is kept as our analysis may shed light on its nature. All of the sources from Soszynski et al. (2019) are in the `vari_cepheid` table, except OGLE-LMC-CEP-4689. This is the well known variable HV 2827, listed in the *Gaia* main catalogue but not in the *Gaia* cepheid and `vari_summary` tables. The source is kept.
Thirty-one sources from the `vari_cepheid` table are not in the samples from Pietrukowicz et al. (2021) and Soszynski et al. (2019).
The 55 sources are matched with the SIMBAD database to obtain additional names and identifiers. One additional source in the SMC (for a total of seven) and one in the LMC (for a total of nine) is in the sample (probably they are located outside the OGLE footprint). Twelf objects are likely members of M31 and seven are likely members of M33. The remaining 20 appear to be in the Milky Way. Five of them are in the direction of the Galactic Bulge and four of these have been classified as T2C by the OGLE team. In total 10 of objects in the MW have alternatively been classified as T2Cs.
All LMC objects except one, and all SMC objects except two were studied by GL23, while two were studied in G20. The analysis of the SEDs is repeated here independently however. There are known CCs in other galaxies with periods longer than 50 days, see e.g. Musella (2022) but they happen not to be included in the *Gaia* `vari_cepheid` table.
The spectral energy distributions (SEDs) are constructed using photometry retrieved mostly, but not exclusively, via the VizieR web-interface. This includes GALEX, various OGLE catalogues, Gaia DR3 photometry, *HST* F555W, F814W, and F160W photometry infrared data from the VMC/VVV and VHS surveys, and Akari, *Spitzer* IRAC and MIPS, and CatWISE and AllWISE photometry at the longest wavelenghts. Whenever possible the magnitudes at mean light were taken.

The Modelling

The SEDs are fitted with the code More of DUSTY (MoD, Groenewegen (2012) which uses a slightly updated and modified version of the DUSTY dust radiative transfer (RT) code (Ivezic et al. 1999) as a subroutine within a minimisation code. Initially the dust optical depth is initially set to zero. In that case the input to the model are the distance, reddening, and a model atmosphere. For the LMC, M31 and M33 mean distances from the literature were adopted and a geometric correction was applied. The depth effect in the SMC is considerable, e.g. Ripepi et al. (2017), and all SMC sources have been adopted to be at the mean distance. For the Galactic Bulge region (defined as the region with $266 < R.A. < 270^\circ$ and $-33 < Dec < -28^\circ$ and compromising of five sources) the distance from the GRAVITY experiment have been adopted. For the remainder of the MW sources the geometric distance from Bailer-Jones et al. (2021) has been adopted, see the Table.

Region	Distance model (kpc)	References
M33	840 ± 11 + geometric correction	Breuval et al. (2023), Kourkchi et al. (2020)
M31	761 ± 11 + geometric correction	Li et al. (2021), Dalcanton et al. (2012)
LMC	49.59 ± 0.55 + geometric correction	Pietrzynski et al. (2019), Riess et al. (2019)
SMC	62.44 ± 0.94	Graczyk et al. (2020)
BUL	8.28 ± 0.03	GRAVITY Collaboration (2021, 2022)
MW	see text	-

The 3D reddening maps of Lallement et al. (2022) and Vergely et al. (2022) were used to obtain the $A_{\rm V}$ in a given direction as well as the distance to which this reddening refers. For the sources in M31 and M33 a value of $A_{\rm V} = 0.17$ has been adopted which is the average value from the 3D reddening map at the largest available distance in the direction of those galaxies. For the MCs the reddening map of Skowron et al. (2021) is used and the $E(V-I)$ value in the map closest to the source is taken.

MARCS model atmospheres are used as input (Gustafsson et al. 2008) for $\log g = 1.5$ and metallicity -0.50 and -0.75 dex for the LMC and SMC stars, and $+0.00$ for M31, M33 and MW sources, respectively.

For every model atmosphere (that is, effective temperature) a best-fitting luminosity (with its [internal] error bar, based on the covariance matrix) is derived with the corresponding reduced chi-squared of the fit. The model with the lowest $\chi^2_{\rm r}$ then gives the best-fitting effective temperature. Considering models within a certain range above this minimum $\chi^2_{\rm r}$ then gives the estimated error in the effective temperature and luminosity. For the luminosity this error is added in quadrature to the internal error in luminosity. In the model fitting procedure photometric outliers are excluded in the following way. The photometric error bar for each data point was added in quadrature to 1.486 · median absolute deviation (MAD) of the residuals in the fit to give a σ. If the absolute difference between model and observations was larger than 4σ the point was flagged and plotted with an error bar of 3.0 mag to still identify it but to have no influence on the fitting. The model grid over temperatures was run again, and the clipping procedure repeated. Then the run over effective temperatures was repeated a last time.
For eight sources the SED suggested that an NIR excess is present. In those cases the models were re-run, adding the dust temperature and the inner radius and the dust optical depth as two additional free parameters (and assuming spherical symmetry). The dust composition was taken to that used in G20, namely a dust largely composed of metallic iron.
The Figure below shows some the fits that can be obtained for two stars assuming no dust (only the stellar atmosphere) and including dust.

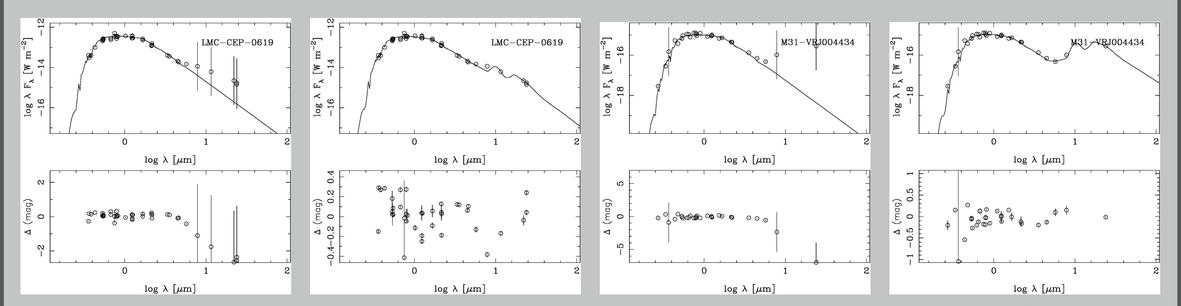

Figure 1: Examples of fits to the SEDs without and with assuming dust. The upper panels show the observations (with error bars) and the model. The lower panel shows the residuals. Outliers have been plotted with an (arbitrary) error bar of 3.0 mag.

The Results

Figure 2 shows the Hertzsprung-Russell diagram together with sets of evolutionary tracks and ISs, see a detailed explanation in the caption regarding the meaning of the symbols, colours, and lines. Overall there is a very good agreement between the position of the CCs in the sample and the theoretical instability strips, but for about 15 objects (all in the MW or Bulge) the position suggests a T2C nature. Plotting the best models with or without dust in the HRD does not make any significant difference.

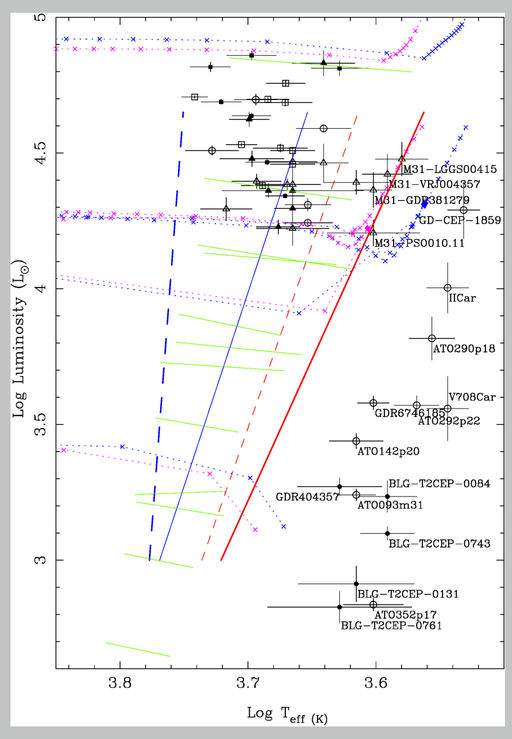

Figure 2. The Hertzsprung-Russell diagram. The left-hand panel presents an overview while the red-hand panel gives focusses on the T2Cs. Symbols are follows: filled squares (SMC), open squares (LMC), open triangles (M31), filled triangles (M33), filled circles (Galactic Bulge), and open circles (MW). Stars located outside the bulk of objects are are identified. Blue and red lines indicate the blue and red edge of the IS. The results from De Somma et al. (2021) are plotted for $Z = 0.03$ (as thick solid lines) and $Z = 0.004$ models (as thinner dashed lines), respectively, for their type A mass-luminosity relation. Green lines indicate evolutionary models from Anderson et al. (2016). Increasing in luminosity are tracks for initial mass (number of the crossing through the IS): 4 (1), 5 (1), 5 (2), 5 (3), 7 (1), 7 (2), 7 (3), 9 (1), 9 (2), 9 (3), 12 (1), 15 $M_\odot$ (1). The blue and pink crosses indicate MIST evolutionary tracks for $v/v_{\rm crit} = 0.4$ for 10 and 17 $M_\odot$ (and [Fe/H]= 0.0 dex) and 9 and 15 $M_\odot$ (and [Fe/H]= −0.50 dex), respectively, plotted at 10^4 year intervals.

As a check on the possibility that the IR excess is associated to the CCs and not related to other emission images from the ALLWISE survey (`https://irsa.ipac.caltech.edu/applications/wise/`) and Spitzer Enhanced Imaging Products (SEIP; `https://irsa.ipac.caltech.edu/data/SPITZER/Enhanced/SEIP/`) were inspected. The Figures show W1 and W3, and IRAC 1 and 4 images, respectively, around selected the 8 CCs where the SEDs suggested the presence of an IR excess.
For the Galactic cepheid II Car and the one in the LMC the fields are "clean" and the IR excess is likely associated to the star. For most of the others the IRAC 1 (3.6 μm) field is clean, but the emssion at 8.0 μm and in the two WISE filters is often not detected or clearly confused or blended.

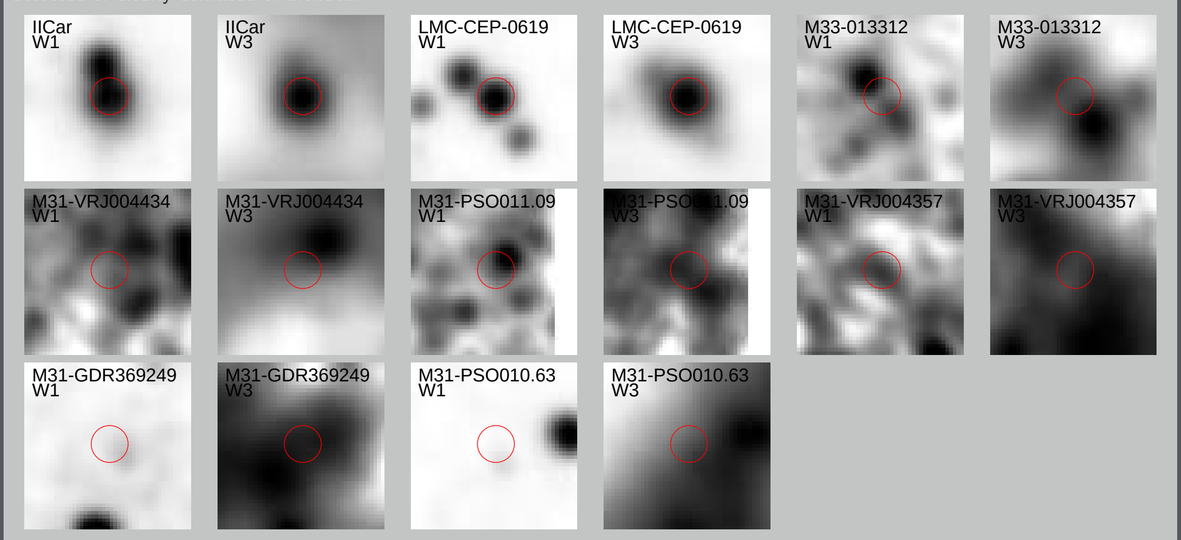

Figure 3: Cut-outs of about 1′x 1′ (45x45 pixels of 1.37″) in the W1 and W3 filters centered on the CC. Cutlevels are at the 0.5 and 99.5% level. The red circle marks the nominal position and has a radius of 5 pixels, approximately 1 FWHM of the point spread function.

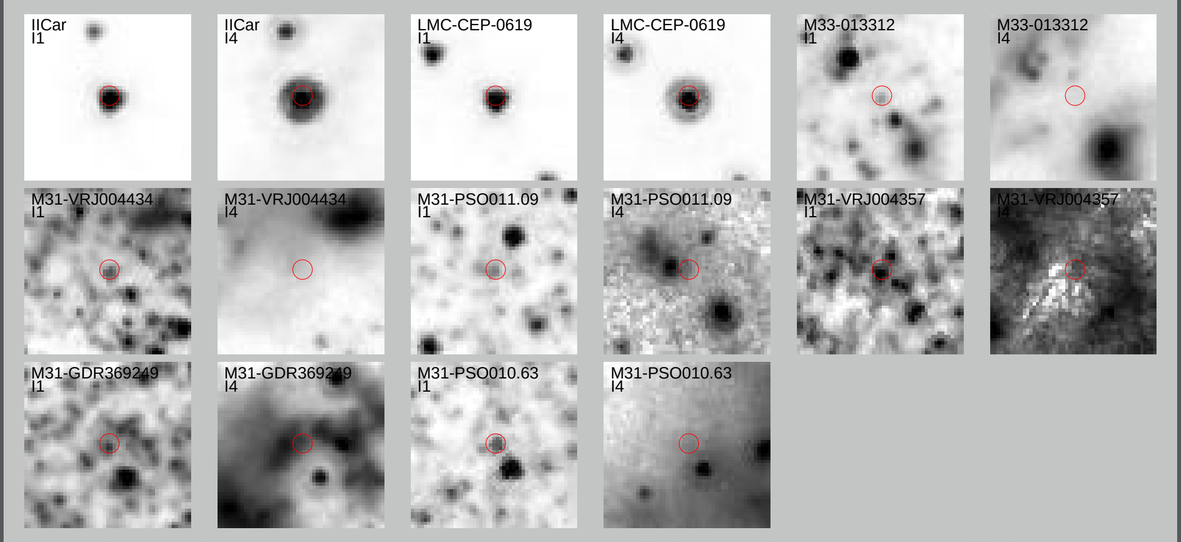

Figure 4: Cut-outs of about 30″ x 30″ (51x51 pixels of 0.60″) in the IRAC 1 and 4 filters centered on the CC. Cutlevels are at the 0.5 and 99.5% level. The red circle marks the nominal position and has a radius of 3 pixels, approximately 1 FWHM of the point spread function.

The Conclusions

In G20 and GL23 a large number of SEDs of CCs in the MW and in the MCs was fitted. In the MW about 5% was found to have an IR excess, in the LMC only 1 in 142 and 0/77 in the SMC. The poster presents additional work on 55 CCs with periods longer than 50 days in the MW, the MCs, M31 and M33. One additional star with likely NIR excess in found in the MW, and the one LMC star found in GL23 is confirmed. For the stars in M31 and M33 inspection of the IRAC and WISE images shows that the MIR excess is very likely not associated to the star.
Can NIR excess have an impact on the calibration of the *PL*-relation of classical cepheids? Probably not, but a definitive answer remains difficult to give. Direct interferometric observations in the optical or NIR are impossible for objects in the MCs, and the SED modelling has limitations as there is typically less data available at the longest wavelengths for the MC objects. One way forward is to take MIR spectra of candidate objects to look for any dust feature in the 10 μm region or at least characterise the (near featureless) continuum.

The References

- Anderson, Saio, Ekström, et al. 2016, A&A 591, A8
- Bailer-Jones, Rybizki, Fouesneau, Demleitner & Andrae 2021, AJ 161, 147
- Bird, Stanek, & Prieto 2009, ApJ 695, 874
- Breitfelder, Merand, Kervella, et al. 2016, A&A 587, A117
- Breuval, Riess, Macri, et al. 2023, ApJ 951, 118
- Dalcanton, Williams, Lang, et al. 2012, ApJS 200, 18
- De Somma, Marconi, Cassisi, et al. 2021, MNRAS 508, 1473
- Graczyk, Pietrzynnski, Thompson, et al. 2020, ApJ 904, 13
- Gallenne, Kervella & Merand, 2012, A&A 538, A24
- Gallenne, Merand, Kervella, et al. 2013, A&A 558, A140
- Gallenne, Kervella, Merand, et al. 2017, A&A 608, A18
- GRAVITY Collaboration, Abuter, Aimar, et al. 2022, A&A 657, L12
- GRAVITY Collaboration, Abuter, Amorim, et al. 2021, A&A 647, A59
- Groenewegen 2012, A&A 543 A36
- Groenewegen 2020, A&A 635, A33
- Groenewegen & Jurkovic, 2017, A&A 604, A29
- Groenewegen & Lub 2023, A&A 676, A136
- Gustafsson, Edvardsson, Eriksson, et al. 2008, A&A 486, 951
- Ivezic, Nenkova, & Elitzur, M. 1999, DUSTY: Radiation transport in a dusty environment, Astrophysics Source Code Library
- Kervella, Merand, Perrin, & Coude du Foresto, 2006, A&A, 448, 623
- Kourkchi, Courtois, Graziani, et al. 2020, AJ 159, 67
- Li, Riess, Busch, et al. 2021, ApJ 920, 84
- Merand, Kervella, Coude du Foresto, et al. 2006, A&A, 453, 155
- Musella 2022, Universe, 8, 335
- Musella, Marconi, Molinaro, et al. 2021, MNRAS, 501, 866
- Lallement, Vergely, Babusiaux & Cox 2022, A&A 661, A147
- Madore, 1982, ApJ 253, 575
- Ripepi, Cioni, Moretti, et al. 2017, MNRAS, 472, 808
- Nardetto, Merand, Mourard, et al. 2016, A&A, 593, A45
- Pietrzynski, Graczyk, Gallenne, et al. 2019, Nature 567, 200
- Pietrukowicz, Soszynski & Udalski 2021, AcA, 71, 205
- Riess, Casertano, Yuan, Macri, & Scolnic, D. 2019, ApJ 876, 85
- Riess, Yuan, Macri, et al. 2022, ApJ 934, L7
- Ripepi, Clementini, Molinaro, et al. 2023, A&A, 674, A17
- Soszynski, Udalski, Szymanski et al. 2019, AcA, 69, 87
- Skowron, Skowron, Udalski, et al. 2021, ApJS 252, 23
- Trahin B. 2019, PhD thesis, L'Universite PSL, l'Observatoire de Paris
- Trahin B., Breuval, Kervella, et al. 2021, A&A, 656, A102
- Vergely, Lallement, & Cox 2022, A&A 664, A174

martin.groenewegen@oma.be